Mechanical force-mediated cellular crosstalk maintains the integrity of the lung gas exchange niche

Chen Shen[1,2], Michael P. Morley[1,2,3], Gan Zhao[1,2], Dakota L. Jones[1,2], Sarah E. Schaefer[1,2], Joseph D. Planer[1,2], Ullas V. Chembazhi[1,2], Mijeong Kim[1,2], Yun Ying[1,2], Su Zhou[1,2], Shanru Li[1,2], Hannah Hallquist[1,2], Ana Lange[1,2], Maria C. Basil[1,2,3], Edward E. Morrisey[1,2,3,4,*]

[1]Department of Medicine, Perelman School of Medicine, University of Pennsylvania, Philadelphia, PA, USA.

[2]Penn-CHOP Lung Biology Institute, Perelman School of Medicine, University of Pennsylvania, Philadelphia, PA, USA.

[3]Penn Cardiovascular Institute, University of Pennsylvania, Philadelphia, PA, USA.

[4]Department of Cell and Developmental Biology, Perelman School of Medicine, University of Pennsylvania, Philadelphia, PA, USA.

***Corresponding author:**

Edward E. Morrisey
Department of Medicine
University of Pennsylvania
Smilow Translational Research Center, Room 11-124
3400 Civic Center Blvd
Philadelphia, PA 19104-5129
Email: emorrise@pennmedicine.upenn.edu

Abstract

The lungs undergo constant mechanical strain as part of their function. Within the lung alveoli, alveolar epithelial type 1 (AT1) cells and associated capillary endothelial cells (CAP) comprise the minimal gas exchange unit. How cells in the alveolar niche respond to respiration-mediated mechanical forces remains poorly understood. Using a reversible bronchial ligation model to control unilateral lung motion in mice, we show that blocking respiratory movements in the lungs leads to transcriptional changes in signaling involved in dysfunctional lung repair. Inhibited lung motion induces the emergence of a permanent, distinct mechanically induced capillary endothelial CAP or (miCAP) state, defined by expression of *Ntrk2*. Importantly, the emergence of miCAPs requires attenuated mechanotransduction signaling in adjacent AT1 cells. Normalization of lung motion after respiratory blockade spontaneously activates the proliferation of miCAPs, while other transcriptional changes are maintained. Collectively, these results reveal a mechano-responsive endothelial cell state induced by respiration mechanics and mechanosensing in adjacent AT1 cells, revealing the distinct impact of mechanical strain on the lung gas exchange interface.

Introduction

Pulmonary gas exchange occurs within the alveoli, the elastic air sacs in the distal lung[1, 2]. During respiration, the alveoli are subjected to a constant, cyclical mechanical strain, which facilitates gas diffusion across a tight interface formed by the alveolar epithelium and the endothelium of the adjacent capillary plexus, with a fused basement membrane in between[2, 3]. In lung diseases, this mechanical load is often disrupted, represented by damaged alveolar tissue architecture and compliance[4]. Despite the importance of maintaining pulmonary mechanical homeostasis, how cells within the alveolar niche respond to mechanical cues and consequently regulate lung tissue structure and function remains poorly understood. Previous *in vivo* studies have been largely limited to observations using transgenic mice with conditional deletion of genes crucial for the mechanosignaling transduction, in which the cyclical lung motion remains uninterrupted[5]. Recently, our group developed a bronchial ligation procedure that allows unilateral restriction of lung motion in mouse[6]. Using this model, we demonstrated that alveolar type I (AT1) epithelial cells are responsive to respiration-mediated mechanical forces. AT1 cells reprogrammed into alveolar type II (AT2) epithelial cells with surgical blockade of lung motion[6]. Similar AT1 cell reprogramming was noted when inhibiting mechanotransduction in AT1 cells using transgenic mouse models inhibiting Hippo signaling and actin dynamics, highlighting the importance of mechanical forces in AT1 cell fate maintenance[6, 7].

In addition to alveolar epithelial cells, whether and how other cells within the lung can sense and respond to respiration-mediated mechanical cues is not well understood. Here, we have advanced the bronchial ligation model to investigate mechanical force-induced alterations in cell state/fate and behavior in a reversable manner. Single cell analyses of ligated mouse lungs revealed transcriptomic differences in multiple cell types in response to respiratory blockade, with capillary endothelial cells (CAPs) showing dramatic changes. We found a distinct ligation-induced CAP state, marked by high *Ntrk2* expression, and have named it mechanically induced CAPs or miCAPs. These miCAPs share certain gene expression hallmarks with the previously identified acute lung injury-induced CAPs (iCAPs)[8] and require the attenuation of mechanosignaling in AT1 cells to emerge. miCAPs also exhibited enhanced proliferation in response to elevated mechanical forces. Reversing the bronchial ligation model and allowing normalization of lung motion shows that the miCAP state persists even after restored respiratory motion. Together, our findings reveal that respiration-mediated mechanical forces are important for maintaining the homeostasis of the lung gas exchange interface, with AT1 cells transmitting signals to adjacent cells to regulate alveolar homeostasis.

Results

Mechanical forces maintain homeostasis of multiple lung cell lineages

To understand how respiration-mediated mechanical forces regulate cells in the lung, we used a bronchial ligation model, where the left main bronchus of mice is ligated by a removable micro-clip to temporarily restrain unilateral respiratory movements (Figure 1A). We performed sham or bronchial ligation surgery in adult wildtype CD1 mice, isolated cells from the mouse lungs, and performed single-cell RNA sequencing (scRNA seq) to determine transcriptomic changes in cells due to inhibited respiration (Figure 1A). We successfully identified all expected cellular compartments (Figure 1B) and cell types (Supplementary figure 1A-B). To determine the mechanosignaling changes in each cell compartment, we created a mechanoregulation score for each cell based on the expression profile of 47 genes that are important for mechanotransduction (Figure 1C). We found that the mechanoregulation score of pulmonary cell compartments showed a divergent change in response to bronchial ligation, with the epithelium being most significantly decreased (Figure 1C), suggesting lung epithelial cells are sensitive to respiration-mediated mechanical forces.

Next, we performed a gene set enrichment analysis to identify the biological processes specific to the bronchial ligation procedure. Various events that control cell motility were upregulated in response to lung motion inhibition, including axoneme assembly, cilium organization, microtubule-based movement, and cell projection assembly (Figure 1D). Cell machineries that are associated with tissue repair were found to be suppressed by bronchial ligation, suggesting cyclical mechanical strain during respiration is critical for lung tissue repair (Figure 1D). Wnt signaling, a pivotal pathway regulating lung tissue repair and regeneration[9, 10], was downregulated by respiratory blockade (Figure 1D). These results collectively indicate that respiration-mediated mechanical forces are required for pulmonary homeostasis.

Inhibited lung motion induces differential transcriptional responses in various cell lineages in the lung

We noted a transcriptional difference between ligated mouse lungs and controls in various cell types (Supplementary figure 1C). To investigate cell state changes in depth, we subseted cells from each lineage, reclustered them, and performed informatic analyses at a higher resolution. No significant transcriptional differences were observed in the alveolar epithelial cells (Supplementary figure 2A-B). However, we noticed a remarkable loss of AT1 cells in the ligated mouse lung scRNA seq (Supplementary figure 2C). We validated the loss of AT1 cells by tissue immunostaining and showed that the percentage of HOPX$^+$ AT1 cells was significantly reduced in response to bronchial ligation, while that of LAMP3$^+$ AT2 cells was increased (Supplementary figure 2D-F). This is consistent with our previous findings that bronchial ligation induces AT1 cell reprogramming into AT2 cells[6].

Within pulmonary mesenchyme, bronchial ligation caused a transcriptional change in alveolar fibroblasts (Supplementary figure 3A-B), marked by the expression of various genes, some of which were reported to be associated with lung fibrosis including *Slc12a2*[11] and *Ltbp2*[12] (Supplementary figure 3C-D). In the myeloid compartment, we noted the altered single cell transcriptome of alveolar macrophages (aMAC) in ligated mouse lungs labeled by high level of *Cd63* and *Inhba* (Supplementary 4A-D). No significantly transcriptional differences were observed in lymphoid cells (Supplementary 4E-F).

A transcriptionally distinct CAP state arises upon inhibited lung motion

Mechanical stress due to ventilation-induced lung injury leads to damage of pulmonary endothelial structure and function[13]. Our scRNA seq analyses showed the emergence of a distinct capillary

endothelial cell (CAP) state in mouse ligated lungs compared to the control (Figure 2A). We call these cells mechanically induced CAPs or miCAPs (Figure 2B-C). The miCAPs are characterized by enriched expression of genes including *Ntrk2* and *Sparcl1* in addition to lineage markers of the progenitor CAP1s[14, 15] such as *Gpihbp1* (Figure 2D and Supplementary figure 5A-D). We isolated cells from sham or ligated mouse lungs and performed flow cytometry analyses using a Tropomyosin receptor kinase B (TrkB) antibody to quantitate the percentage of *Ntrk2*$^{+}$ miCAPs. We confirmed that attenuated respiration by bronchial ligation led to the emergence of miCAPs in mouse lungs, occupying approximately 40% of the total lung endothelial cell (EC) population (Figure 2E and Supplementary figure 6A). In addition, immunohistochemistry (IHC) results also validated the presence miCAPs in mouse ligated lungs (Figure 2F).

To further characterize these miCAPs, we performed a comparative gene set enrichment analysis between miCAPs and other CAPs. Cell division processes were downregulated in miCAPs (Figure 2G). We further examined miCAP proliferation by detecting 5-ethynyl-2'-deoxyuridine (EdU) incorporation in cells (Figure 2H) and found that compared to ECs from sham mouse lungs or TrkB^{-} ECs from the same ligated lungs, the proliferation of miCAPs was significantly reduced (Figure 2I and Supplementary figure 7A). This suggests that miCAPs are quiescent upon blockade of lung motion. We also noted that miCAPs express lower level of genes involved in cell migration, DNA repair, and angiogenesis (Figure 2G), indicating these cells might demonstrate impaired endothelial function.

Development of miCAP fate is independent of endothelial cell intrinsic mechanosignaling

To investigate the cell of origin for the miCAPs, we utilized two previously validated CAP lineage trace mouse lines[8], *Kit*^{MerCreMer}*; R26R*^{tdTomato} and *Car4*^{CreERT2}*; R26R*^{tdTomato}, to lineage label CAP1s and CAP2s, respectively, and track their cell state changes upon attenuated respiratory movements (Figure 3A). CAP1- and CAP2-trace mice were given tamoxifen to initiate lineage tracing, followed by sham or bronchial ligation surgery (Figure 2A). Flow cytometry and IHC analyses indicated that both CAP1 and CAP2 lineage gave rise to miCAPs upon inhibition of respiratory motion (Figure 3B-C and Supplementary figure 8A).

During breathing movements, the capillary plexus undergoes constant biophysical strain such as stretching and shear stress, which maintains the integrity of the capillary barrier[16, 17]. Thus, we determined whether the miCAP state is caused by aberrant mechanosignaling activity in CAPs. Mouse lines were created to block intrinsic mechanotransduction in either CAP1 or CAP2 by

conditional knockout of *Cdc42,* the pivotal component of cytoskeletal mechanosignaling (Figure 3D) [18]. These knockouts successfully attenuated mechanotransduction in CAPs, indicated by decreased expression of mechanosignaling target genes including *Ccn1*, *Ccn2* and *Ankrd1*[19-21] (Supplementary figure 8B). Surprisingly, we did not observe miCAPs emerging from either CAP1 or CAP2 lineage upon inhibited mechanotransduction in these CAPs (Figure 3E). These results suggest that blocking cell intrinsic mechanosignaling in CAPs is not sufficient to activate the miCAP state.

The emergence of miCAPs requires AT1 cell mechanosensing

We previously demonstrated that AT1 cells are sensitive to respiration-mediated mechanical forces[6]. Inhibition of respiratory movements by bronchial ligation or loss of *Cdc42* in AT1 cells causes them to reprogram into AT2 cells[6]. Functionally, AT1 cells form a delicate interface with the capillary plexus to facilitate gas exchange[1-3]. Therefore, we hypothesized that respiration-mediated mechanical regulation of AT1 cells might be essential to maintain the proper cellular homeostasis in neighboring CAPs. To test this hypothesis, we isolated cells from control mouse lungs or those with *Cdc42* knockout in AT1 cells ($Cdc42^{AT1\text{-}KO}$) and performed a scRNA seq experiment to assess changes in cell state (Figure 4A). Similar to bronchial ligation, $Cdc42^{AT1\text{-}KO}$ induced a remarkable transcriptional change in CAPs (Figure 4B-C). We reannotated the CAPs in our scRNA seq data and showed that this CAP population specific to $Cdc42^{AT1\text{-}KO}$ mouse lungs (AT1-induced CAP) expressed high levels of *Ntrk2* (Figure 4D). Although the AT1-induced CAPs did not express some of other miCAP marker genes, such as *Sparcl1* (Figure 4D), there was a strong statistically significant correlation between the transcriptome of these cells and that of miCAPs, indicating they represent similar cell states (Figure 4E). Therefore, we also call these cells miCAPs hereafter. The existence of miCAPs in $Cdc42^{AT1\text{-}KO}$ mouse lungs was further validated by flow cytometry and tissue immunostaining using TrkB antibody (Figure 4F-G). Collectively, these data support the concept that AT1 cells are a node of mechanotransduction in the gas exchange niche that can transmit their mechanosensitive responses to adjacent CAPs to cause the emergence of miCAPs (Figure 4H).

miCAPs are sensitive to mechanical forces

We next investigated whether this miCAP state reflects a permanent change in endothelial cell state or transient due to temporarily restricted respiration. Two weeks after bronchial ligation, a secondary surgery was performed in the mice to remove the clip blocking respiratory motion in the left lung (Figure 5A). Lung reinflation was assessed using microCT scans and lungs appeared

normal after clip removal (Figure 5B). We did not note tissue structural damage or changes in immune cell infiltration in mouse lungs after clip removal compared to sham (Supplementary figure 9A-B). Of note, the cellular composition of alveolar epithelium returned to normal after restored lung motion (Supplementary 10A-C), supporting the normalization of epithelial composition in the reinflated lungs. scRNA seq analyses showed that despite restoration of respiratory motion (Figure 5B and Supplementary figure 11A), miCAPs still existed in the mouse lungs after clip removal (Figure 5C). We also noted a significant number miCAPs in mouse lungs with reversed ligation by miCAP flow cytometry or immunostaining for TrkB (Figure 5D-E), suggesting this miCAP state is a persistent endothelial state change. Examination of the transcriptional signature of miCAPs revealed a restoration of endothelial function after lung motion rescue, including endothelial cell proliferation, migration, and angiogenesis (Supplementary figure 11B). Interestingly, rescue of lung motion significantly promoted the proliferation of miCAPs to a level comparable to control ECs, while the proliferation of TrkB^{-} ECs did not show a difference in response to altered respiratory motion (Figure 2I and 5F-G). These findings highlight that miCAPs are the subset of endothelial cells that are responsive to mechanical cues within the lung.

Discussion

Despite the importance of respiration-mediated mechanical forces in lung gas exchange function, how they impact cells within the lung is little known due to a lack of appropriate *in vivo* model to study such mechanical load. In this study, we leveraged a bronchial ligation model and defined transcriptional changes in pulmonary cells using scRNA seq. Different pulmonary cell compartments showed heterogenous responses to inhibited lung motion, with epithelial cells being the most sensitive, particularly AT1 cells. AT1 cells require respiratory movements to maintain their cell fate[6]. Here we further demonstrated that altered mechanosignaling in AT1 cells could also impact the fate of neighboring endothelial cells to induce a miCAP state, suggesting AT1 cells are the primary mechanical sensor in the distal lung and signal to other cells to control the homeostasis of the alveolar niche. This also highlights the importance of intercellular communication during lung mechanics, in addition to individual cell lineage's responses. In other lung injury models, it has been shown that different cell types coordinate tissue repair and regeneration[22-24]. Such mechanisms might also play a key role in maintaining the mechanical environment within the lung.

AT1 cells cover over 90% of the alveolar surface, acting as a major player in lung gas exchange[2]. The large, flat, stretchy cell morphology reflects high mechanical activity in these cells[2, 6, 7, 25]. The

percentage of AT1 cells is decreased in ligated mouse lungs, however, it remains unchanged in *Cdc42*$^{AT1-KO}$ lungs[6]. In addition, the cyclical lung motion is unperturbed in *Cdc42*$^{AT1-KO}$ animals. These indicate that the emergence of miCAPs is driven by altered mechanotransduction activity within AT1 cells, but not the decrease in AT1 cell number or loss of cyclical lung motion. These data also suggest that maintaining the proper ratio of AT1 and AT2 cells requires mechanical signaling throughout the alveolar niche, which is disrupted in the bronchial ligation model but not in *Cdc42*$^{AT1-KO}$ lungs. We previously demonstrated that AT1 reprogramming into AT2 cells is dependent on actin-mediated AT1 cell stretch[6]. Our current work further supports the critical role of proper actin cytoskeleton organization within AT1 cells in maintaining lung tissue homeostasis, particularly the integrity of lung gas exchange interface. The mechanosignaling-dependent, morphological change of AT1 cells might drive an altered physical interaction between them and neighboring cells such as CAPs to modulate the fate of cells within the alveolar niche.

The miCAPs we identified in both bronchial ligation and *Cdc42*$^{AT1-KO}$ models highly express *Ntrk2*. *Ntrk2* encodes TrkB protein, which is required for tactile sensation of neurons and regulates behavior and function of neuronal cells[26-30]. It remains possible that TrkB in miCAPs also plays a role in sensing tactility with the surrounding mechanical environment including AT1 cells and extracellular matrix. While *Ntrk2* is a consistent marker of miCAPs induced by bronchial ligation and *Cdc42*$^{AT1-KO}$, we note a divergence the expression of other genes between these two models including *Sparcl1,* which may be due to the finding that *Sparcl1* in lung ECs induces a pro-inflammatory macrophage state during acute viral lung injury[24]. This correlates with our previous work showing that an acute lung injury-induced CAP state (iCAPs) that emerges after influenza based acute lung injury also highly express both *Ntrk2* and *Sparcl1*[8]. Thus, we anticipate that the upregulated endothelial *Sparcl1* expression might result from injury-associated inflammation.

The development of a reversible bronchial ligation procedure allowed us to examine how persistent the changes that occur upon blockade of respiratory motion are. Our findings using reversible bronchial ligation showed that alveolar epithelial cell ratios are normalized after restoring motion in the ligated mouse lungs, suggesting that appropriate levels of mechanotransduction are critical for AT2 differentiation. This also highlights the application of this surgical model to investigate lung tissue repair and regeneration in the context of mechanotransduction. While complex disease pathology confounds the ability to determine how cellular processes are impacted by alterations in mechanotransduction, our reversible ligation model adds an important new tool to explore these cellular changes in lung injury and disease.

The miCAP state persists through the lung motion rescue and we find these cells spontaneously respond to normalization of respiration-mediate mechanical forces by becoming more proliferative, suggesting these cells may act as a potential progenitor during the endothelial regeneration process. Future functional studies on miCAPs in reversible bronchial ligation and lung disease models will provide critical insights into how pulmonary endothelium contributes to lung tissue repair and regeneration.

References

1. Knudsen L, Ochs M. The micromechanics of lung alveoli: structure and function of surfactant and tissue components. Histochem Cell Biol. 2018;150(6):661-76. Epub 20181102. doi: 10.1007/s00418-018-1747-9. PubMed PMID: 30390118; PMCID: PMC6267411.
2. Weibel ER. Lung morphometry: the link between structure and function. Cell Tissue Res. 2017;367(3):413-26. Epub 20161216. doi: 10.1007/s00441-016-2541-4. PubMed PMID: 27981379.
3. Zepp JA, Morrisey EE. Cellular crosstalk in the development and regeneration of the respiratory system. Nat Rev Mol Cell Biol. 2019;20(9):551-66. Epub 20190619. doi: 10.1038/s41580-019-0141-3. PubMed PMID: 31217577; PMCID: PMC7254499.
4. Pride NB, Macklem PT. Lung Mechanics in Disease. Comprehensive Physiology. p. 659-92.
5. Tschumperlin DJ, Ligresti G, Hilscher MB, Shah VH. Mechanosensing and fibrosis. J Clin Invest. 2018;128(1):74-84. Epub 20180102. doi: 10.1172/JCI93561. PubMed PMID: 29293092; PMCID: PMC5749510.
6. Shiraishi K, Shah PP, Morley MP, Loebel C, Santini GT, Katzen J, Basil MC, Lin SM, Planer JD, Cantu E, Jones DL, Nottingham AN, Li S, Cardenas-Diaz FL, Zhou S, Burdick JA, Jain R, Morrisey EE. Biophysical forces mediated by respiration maintain lung alveolar epithelial cell fate. Cell. 2023;186(7):1478-92 e15. Epub 20230303. doi: 10.1016/j.cell.2023.02.010. PubMed PMID: 36870331; PMCID: PMC10065960.
7. Penkala IJ, Liberti DC, Pankin J, Sivakumar A, Kremp MM, Jayachandran S, Katzen J, Leach JP, Windmueller R, Stolz K, Morley MP, Babu A, Zhou S, Frank DB, Morrisey EE. Age-dependent alveolar epithelial plasticity orchestrates lung homeostasis and regeneration. Cell Stem Cell. 2021;28(10):1775-89 e5. Epub 20210510. doi: 10.1016/j.stem.2021.04.026. PubMed PMID: 33974915; PMCID: PMC8500919.
8. Niethamer TK, Planer JD, Morley MP, Babu A, Zhao G, Basil MC, Cantu E, Frank DB, Diamond JM, Nottingham AN, Li S, Sharma A, Hallquist H, Levin LI, Zhou S, Vaughan AE, Morrisey EE. Longitudinal single-cell profiles of lung regeneration after viral infection reveal persistent injury-associated cell states. Cell Stem Cell. 2025;32(2):302-21 e6. Epub 20250115. doi: 10.1016/j.stem.2024.12.002. PubMed PMID: 39818203; PMCID: PMC11805657.
9. Aros CJ, Pantoja CJ, Gomperts BN. Wnt signaling in lung development, regeneration, and disease progression. Commun Biol. 2021;4(1):601. Epub 20210520. doi: 10.1038/s42003-021-02118-w. PubMed PMID: 34017045; PMCID: PMC8138018.
10. Zacharias WJ, Frank DB, Zepp JA, Morley MP, Alkhaleel FA, Kong J, Zhou S, Cantu E, Morrisey EE. Regeneration of the lung alveolus by an evolutionarily conserved epithelial progenitor. Nature. 2018;555(7695):251-5. Epub 20180228. doi: 10.1038/nature25786. PubMed PMID: 29489752; PMCID: PMC6020060.
11. Stodberg T, Magnusson M, Lesko N, Wredenberg A, Martin Munoz D, Stranneheim H, Wedell A. SLC12A2 mutations cause NKCC1 deficiency with encephalopathy and impaired

secretory epithelia. Neurol Genet. 2020;6(4):e478. Epub 20200702. doi: 10.1212/NXG.0000000000000478. PubMed PMID: 32754646; PMCID: PMC7357422.
12. Enomoto Y, Matsushima S, Shibata K, Aoshima Y, Yagi H, Meguro S, Kawasaki H, Kosugi I, Fujisawa T, Enomoto N, Inui N, Nakamura Y, Suda T, Iwashita T. LTBP2 is secreted from lung myofibroblasts and is a potential biomarker for idiopathic pulmonary fibrosis. Clin Sci (Lond). 2018;132(14):1565-80. Epub 20180731. doi: 10.1042/CS20180435. PubMed PMID: 30006483; PMCID: PMC6376615.
13. Wang T, Gross C, Desai AA, Zemskov E, Wu X, Garcia AN, Jacobson JR, Yuan JX, Garcia JG, Black SM. Endothelial cell signaling and ventilator-induced lung injury: molecular mechanisms, genomic analyses, and therapeutic targets. Am J Physiol Lung Cell Mol Physiol. 2017;312(4):L452-L76. Epub 20161215. doi: 10.1152/ajplung.00231.2016. PubMed PMID: 27979857; PMCID: PMC5407098.
14. Niethamer TK, Stabler CT, Leach JP, Zepp JA, Morley MP, Babu A, Zhou S, Morrisey EE. Defining the role of pulmonary endothelial cell heterogeneity in the response to acute lung injury. Elife. 2020;9. Epub 20200224. doi: 10.7554/eLife.53072. PubMed PMID: 32091393; PMCID: PMC7176435.
15. Gillich A, Zhang F, Farmer CG, Travaglini KJ, Tan SY, Gu M, Zhou B, Feinstein JA, Krasnow MA, Metzger RJ. Capillary cell-type specialization in the alveolus. Nature. 2020;586(7831):785-9. Epub 20201014. doi: 10.1038/s41586-020-2822-7. PubMed PMID: 33057196; PMCID: PMC7721049.
16. Walsh D, Kostyunina DS, Blake A, Boylan J, McLoughlin P. Shear stress-induced restoration of pulmonary microvascular endothelial barrier function following ischemia reperfusion injury requires VEGFR2 signaling. Am J Physiol Lung Cell Mol Physiol. 2025;328(3):L389-L404. Epub 20241219. doi: 10.1152/ajplung.00200.2024. PubMed PMID: 39701597.
17. Zhong M, Wu W, Kang H, Hong Z, Xiong S, Gao X, Rehman J, Komarova YA, Malik AB. Alveolar Stretch Activation of Endothelial Piezo1 Protects Adherens Junctions and Lung Vascular Barrier. Am J Respir Cell Mol Biol. 2020;62(2):168-77. doi: 10.1165/rcmb.2019-0024OC. PubMed PMID: 31409093; PMCID: PMC6993544.
18. Tapon N, Hall A. Rho, Rac and Cdc42 GTPases regulate the organization of the actin cytoskeleton. Curr Opin Cell Biol. 1997;9(1):86-92. doi: 10.1016/s0955-0674(97)80156-1. PubMed PMID: 9013670.
19. Ma S, Meng Z, Chen R, Guan KL. The Hippo Pathway: Biology and Pathophysiology. Annu Rev Biochem. 2019;88:577-604. Epub 20191219. doi: 10.1146/annurev-biochem-013118-111829. PubMed PMID: 30566373.
20. Dobrokhotov O, Samsonov M, Sokabe M, Hirata H. Mechanoregulation and pathology of YAP/TAZ via Hippo and non-Hippo mechanisms. Clin Transl Med. 2018;7(1):23. Epub 20180813. doi: 10.1186/s40169-018-0202-9. PubMed PMID: 30101371; PMCID: PMC6087706.
21. Wang Y, Xu X, Maglic D, Dill MT, Mojumdar K, Ng PK, Jeong KJ, Tsang YH, Moreno D, Bhavana VH, Peng X, Ge Z, Chen H, Li J, Chen Z, Zhang H, Han L, Du D, Creighton CJ, Mills GB, Cancer Genome Atlas Research N, Camargo F, Liang H. Comprehensive Molecular Characterization of the Hippo Signaling Pathway in Cancer. Cell Rep. 2018;25(5):1304-17 e5. doi: 10.1016/j.celrep.2018.10.001. PubMed PMID: 30380420; PMCID: PMC6326181.
22. Jones DL, Morley MP, Li X, Ying Y, Zhao G, Schaefer SE, Rodriguez LR, Cardenas-Diaz FL, Li S, Zhou S, Chembazhi UV, Kim M, Shen C, Nottingham A, Lin SM, Cantu E, Diamond JM, Basil MC, Vaughan AE, Morrisey EE. An injury-induced mesenchymal-epithelial cell niche coordinates regenerative responses in the lung. Science. 2024;386(6727):eado5561. Epub 20241213. doi: 10.1126/science.ado5561. PubMed PMID: 39666855.
23. Lin SM, Rue R, Mukhitov AR, Goel A, Basil MC, Obraztsova K, Babu A, Crnkovic S, Ledwell OA, Ferguson LT, Planer JD, Nottingham AN, Vanka KS, Smith CJ, Cantu E, 3rd, Kwapiszewska G, Morrisey EE, Evans JF, Krymskaya VP. Hyperactive mTORC1 in lung mesenchyme induces endothelial cell dysfunction and pulmonary vascular remodeling. J Clin

Invest. 2023;134(4). Epub 20231220. doi: 10.1172/JCI172116. PubMed PMID: 38127441; PMCID: PMC10866655.
24. Zhao G, Gentile ME, Xue L, Cosgriff CV, Weiner AI, Adams-Tzivelekidis S, Wong J, Li X, Kass-Gergi S, Holcomb NP, Basal MC, Stewart KM, Planer JD, Cantu E, Christie JD, Crespo MM, Mitchell MJ, Meyer NJ, Vaughan AE. Vascular endothelial-derived SPARCL1 exacerbates viral pneumonia through pro-inflammatory macrophage activation. Nat Commun. 2024;15(1):4235. Epub 20240518. doi: 10.1038/s41467-024-48589-3. PubMed PMID: 38762489; PMCID: PMC11102455.
25. Callaway DA, Penkala IJ, Zhou S, Knowlton JJ, Cardenas-Diaz F, Babu A, Morley MP, Lopes M, Garcia BA, Morrisey EE. TGF-beta controls alveolar type 1 epithelial cell plasticity and alveolar matrisome gene transcription in mice. J Clin Invest. 2024;134(6). Epub 20240111. doi: 10.1172/JCI172095. PubMed PMID: 38488000; PMCID: PMC10947970.
26. Huber K, Kuehnel F, Wyatt S, Davies AM. TrkB expression and early sensory neuron survival are independent of endogenous BDNF. J Neurosci Res. 2000;59(3):372-8. doi: 10.1002/(SICI)1097-4547(20000201)59:3<372::AID-JNR11>3.0.CO;2-F. PubMed PMID: 10679773.
27. Dhandapani R, Arokiaraj CM, Taberner FJ, Pacifico P, Raja S, Nocchi L, Portulano C, Franciosa F, Maffei M, Hussain AF, de Castro Reis F, Reymond L, Perlas E, Garcovich S, Barth S, Johnsson K, Lechner SG, Heppenstall PA. Control of mechanical pain hypersensitivity in mice through ligand-targeted photoablation of TrkB-positive sensory neurons. Nat Commun. 2018;9(1):1640. Epub 20180424. doi: 10.1038/s41467-018-04049-3. PubMed PMID: 29691410; PMCID: PMC5915601.
28. Li Y, Luikart BW, Birnbaum S, Chen J, Kwon CH, Kernie SG, Bassel-Duby R, Parada LF. TrkB regulates hippocampal neurogenesis and governs sensitivity to antidepressive treatment. Neuron. 2008;59(3):399-412. doi: 10.1016/j.neuron.2008.06.023. PubMed PMID: 18701066; PMCID: PMC2655199.
29. Harada C, Guo X, Namekata K, Kimura A, Nakamura K, Tanaka K, Parada LF, Harada T. Glia- and neuron-specific functions of TrkB signalling during retinal degeneration and regeneration. Nat Commun. 2011;2:189. Epub 20110208. doi: 10.1038/ncomms1190. PubMed PMID: 21304518; PMCID: PMC3105320.
30. Klein R, Nanduri V, Jing SA, Lamballe F, Tapley P, Bryant S, Cordon-Cardo C, Jones KR, Reichardt LF, Barbacid M. The trkB tyrosine protein kinase is a receptor for brain-derived neurotrophic factor and neurotrophin-3. Cell. 1991;66(2):395-403. doi: 10.1016/0092-8674(91)90628-c. PubMed PMID: 1649702; PMCID: PMC2710095.
31. Takeda N, Jain R, LeBoeuf MR, Wang Q, Lu MM, Epstein JA. Interconversion between intestinal stem cell populations in distinct niches. Science. 2011;334(6061):1420-4. Epub 20111110. doi: 10.1126/science.1213214. PubMed PMID: 22075725; PMCID: PMC3705713.
32. Chen L, Liao G, Yang L, Campbell K, Nakafuku M, Kuan CY, Zheng Y. Cdc42 deficiency causes Sonic hedgehog-independent holoprosencephaly. Proc Natl Acad Sci U S A. 2006;103(44):16520-5. Epub 20061018. doi: 10.1073/pnas.0603533103. PubMed PMID: 17050694; PMCID: PMC1637614.

Methods

Mouse studies

All mouse experiments were performed following the protocols of the University of Pennsylvania Institutional Animal Care and Use Committee. Adult mice (8-12 weeks old) were used in all the experiments. Cre recombination was initiated by a single dose of tamoxifen (200 mg/kg Sigma-Aldrich) for lineage tracing and 1 dose of tamoxifen (200 mg/kg, Sigma-Aldrich) daily for 3

consecutive days for conditional gene knockout, unless otherwise indicated. Mouse lines used in this study were previously validated and the strains are listed below:

Mouse strain	**Source**	**Catalog#**
CD-1	Charles River	022
Kit^{MerCreMer}	Jackson Laboratory	032052
Car4^{CreERT2}	Morrisey lab	NA
Hopx^{CreERT2} [31]	Jackson Laboratory	017606
R26R^{tdTomato}	Jackson Laboratory	007914
R26R^{EYFP}	Jackson Laboratory	007903
Cdc42^{flox} [32]	Jackson Laboratory	027576

Reversible bronchial ligation

Mice were anesthetized with isoflurane and intubated for ventilation using a MiniVent ventilator (Harvard apparatus; tidal volume of 10 µL per gram mouse body weight, respiratory rate of 150 breaths per minute). The thoracic cavity was exposed by incising 1 cm on the left lateral side of the skin, followed by a 0.5 cm incision at the third left intercostal space. The left main bronchus was clipped using a customized micro vascular clamp (Fine Science Tools Cat#00396-01, jaw dimension = 2 x 1 mm) with a micro clamp applying forceps (Fine Science Tools Cat#00071-14). For clip removal, mice were anesthetized, intubated, and thoracic cavity exposed following the same protocol. An incision was made at the fourth left intercostal space, followed by removal of the clip.

Micro-computed tomography (uCT)

uCT images were generated using a X-Cube CT scanner (Molecubes) located at the Small Animal Imaging Facility at Penn Medicine. Live mice were anesthetized with isoflurane and images were acquired using a respiratory gating approach. The settings for image acquisitation were as follows: reconstructed voxel size: 100 um, X-Ray tube voltage: 50 kVp, X-Ray tube current: 440 uA, exposure time: 32 ms, type of filter used: 0.8 mm aluminum filter, degree of rotation stepping: 0.75 degrees (480 total steps in a 360 degree scan).

Histology

For tissue preparation, mice were euthanized by CO2 inhalation and the lungs were perfused with PBS, followed by inflation with 2% Paraformaldehyde (Thermo Fisher Scientific) at a constant pressure of 25 cm H_2O. Tissues were fixed at 4°C overnight and dehydrated in a series of ethanol

concentration gradients. After dehydration, tissues were embedded in paraffin and sliced into 6 μm thick sections.

Hematoxylin and eosin (H&E) staining was performed as previously described. For immunostaining, the following antibodies were used on paraffin tissue sections:

Antibody	**Source**	**Catalog#**
Goat polyclonal anti-TrkB	Novus Biologicals	AF1494
Mouse monoclonal anti-ERG	Abcam	ab214341
Rabbit monoclonal anti-ERG	Abcam	ab92513
Rabit polyclonal anti-RFP	Rockland	600-401-379
Rat monoclonal anti-LAMP3	Novus Biologicals	DDX0191P-100
Mouse monoclonal anti-HOPX	Santa Cruz	sc-398703
Rabbit monoclonal anti-NKX2.1 (TTF1)	Abcam	ab76013

Imaging and image analysis

H&E stained lung sections were tile-scanned using an EVOS M7000 Imaging System. Fluorescent images were acquired at 20x and 40x using z-stacks on a Zeiss LSM 710 or Leica Stellaris 5 laser scanning confocal microscope. Cell counting analysis was completed within FIJI.

Single cell isolation, flow cytometry, and FACS

Lungs were harvested and digested into single cell suspensions as previously described. For flow cytometry, cells were stained with combination of antibodies (1:200 dilution) listed below:

Antibody	**Source**	**Catalog#**
CD45-PerCP-Cy5.5	Thermo Fisher	45-0451-82
CD31-PE-Cy7	Thermo Fisher	25-0311-82
TrkB-Biotin	R&D systems	BAF1494
Streptavidin-APC	Thermo Fisher	17-4317-82

For FACS of CAP-trace cells, lung cells were incubated with mouse CD45 MicroBeads magnetic beads (Miltenyi Biotec Cat#130-052-301) and the $CD45^+$ population was depleted as per the manufacturer's protocol. $CD45^-$ cells were then incubated with both CD45-APC and CD31-PE-Cy7 at 1:200 dilution and subjected to FACS for isolation of APC^-, $PE\text{-}Cy7^+$, and $tdTomato^+$ cells.

EdU proliferation assay

5-Ethynyl-2'-deoxyuridine (Santa Cruz Biotechnology Cat#sc-284628B) was dissolved in tap water at a concentration of 2 g/L, filtered through a 0.2 μm filter, and stored at 4°C. To create a drinking water solution, this stock solution was diluted to a final concentration of 0.2 g/L in tap water and sterile filtered. Mice consumed EdU water over the time course indicated. EdU incorporation was detected using the Click-iT™ Plus EdU Alexa Fluor™ 488 Flow Cytometry Assay Kit (Thermo Fisher #C10632) according to the manufacturer's protocol.

Quantitative RT-PCR

Total RNA was extracted from sorted CAP-trace cells using a RNeasy Mini Kit (Qiagen Cat#74104), reverse transcribed to cDNA using a SuperScriptTM IV kit (Invitrogen Cat#18091050), and used for quantitative PCR reaction on a QuantStudio 7 PCR System (Applied Biosystems) using specific Taqman Probes (Thermo Fisher) or SYBR-Green primers (Integrated DNA Technologies) as listed below:

SYBR-Green primer	**Sequence**
Cdc42 Forward	5'-GAGAAGCTGAGGACAAGATCTAA-3'
Cdc42 Reverse	5'-CACCATCACCAACAACAACAC-3'
Gapdh Forward	5'-AAATGGTGAAGGTCGGTGTGAACG-3'
Gapdh Reverse	5'-ATCTCCACTTTGCCACTGC-3'
Taqman probe	**Catalog#**
Ccn1	Mm00487498_m1
Ccn2	Mm01192233_g1
Ankrd1	Mm00496512_m1
Gapdh	Mm99999915_g1

scRNA-seq and analysis

To create samples for scRNA-seq that adequately represented both immune and non-immune compartments, we used magnetic activated cell sorting (MACS) to isolate $CD45^+$ and $CD45^-$ cells and recombined them at a ratio of 85% CD45- cells to 15% CD45+ cells. Cells were counted using the Countess II FL Automated Cell Counter (Thermo Fisher) and loaded at a concentration of 800-1000 cells/mL onto a 10X Chromium Controller (10X Genomics) following the manufacturer's instructions. cDNA and sequencing libraries were prepared using 10X Genomics reagents. cDNA and library quality control were performed using an Agilent 2100 Bioanalyzer

using the Bioanalyzer High Sensitivity DNA kit (Agilent #5067-4626). Libraries were then sequenced on an Illumina Novaseq 6000 instrument.

The sequenced data was processed by aligning reads and obtaining unique molecular identifiers (UMIs) using STARsolo (v2.7.11b). Libraries were aligned to a modified mm39 mouse genome. The scRNA-seq data was further processed and analyzed using the Seurat v5 package. Cells which had less than 200, or greater than 5000, detected genes were removed from the analysis. Cells were also removed if the percent mitochondrial reads were greater than 10% and called a doublet using the Scrublet package (https://doi.org/10.1016/j.cels.2018.11.005). Feature (gene) data was scaled in order to removed unwanted sources of variation using the Seurat normalize and scaledata functions based on percent mitochondrial reads, and the number of genes, and total reads. Non-linear dimension reduction was performed using uniform manifold approximation and projections (UMAPs) and Louvain graph-based clustering algorithms.

Marker genes for each celltype were identified using the FindAllMarkers command using the RNA assay within Seurat. Correlation analysis was performed in R and correlation plots made using ggcorrplot. Gene set enrichment analysis (GSEA) of gene ontology (GO) was performed using the 'clusterProfiler' package (DOI: 10.18129/B9.bioc.clusterProfiler). The mechanoregulation gene signature score was calculated based on the gene set 'Mechanoregulation And Pathology Of YAP TAZ Via Hippo And Non Hippo Mechanisms' obtained from Harmonizome 3.0 using the Ucell package (https://doi.org/10.1016/j.csbj.2021.06.043).

Acknowledgements

We thank the Flow Cytometry Core Laboratory at the Children's Hospital of Philadelphia, the Cell and Developmental Biology Microscopy Core at the University of Pennsylvania (UPenn), and the Rodent Cardiovascular Phenotyping Core at the Cardiovascular Institute of UPenn, for their technical assistance. This research was supported by the National Institutes of Health (R01HL164929, R01HL152194, R01HL132999, R01HL162683, R01HL168803 to EEM).

Figure legends

Figure 1: Respiratory restriction induces transcriptional changes in the lung.

A. A schematic of scRNA seq experiment. Cells from wildtype mouse after bronchial ligation or sham surgery were isolated and used for scRNA seq analyses. **B.** A merged UMAP plot of distal lung cells from control and ligated mouse lungs. Cells were annotated by lineage. **C.** A violin plot showing altered mechanical, transcriptional activity by bronchial ligation across pulmonary cell compartments. **D.** Gene set enrichment analysis results showing differential pathways in ligated mouse lungs compared to control.

Figure 2: Respiratory restriction induces a transcriptionally distinct CAP state.

A-B. UMAP plots of CAPs from control and ligated mouse lungs. Cells were annotated by treatment (**A**) or cell type (**B**). **C.** A bar plot showing percentage of each cell type in control or ligated mouse lungs. **D.** A dot plot showing expression of marker genes for each cell type. **E.** Flow cytometry results showing miCAP percentage in indicated lung tissues (n = 5 or 6, mean ± SEM). Asterisks indicate statistical significance (*** p value < 0.001). **F.** Representative IHC images of indicated lung tissues stained with TrkB and ERG, a pan endothelial cell marker (scale bar = 25 μm). **G.** Gene set enrichment analysis results showing pathways specific to miCAPs. **H.** A schematic of flow cytometry experiment determining proliferation in cells. EdU water (0.2 g/L) was provided to mice during indicated time periods. Cells from wildtype mouse after bronchial ligation or sham surgery were isolated and used for flow cytometry. **I.** Flow cytometry results showing proliferating EdU^+ cell percentage in indicated EC populations (n = 5, mean ± SEM). Asterisks indicate statistical significance (* p value < 0.05, ** p value < 0.01).

Figure 3: Development of miCAP fate is independent of endothelial cell intrinsic mechanosignaling.

A. A schematic of CAP lineage trace experiment. CAP1- or CAP2-trace mice were administrated with one dose of tamoxifen, followed by sham or bronchial ligation surgery. Tissues and cells from control or ligated lung were used for imaging or flow cytometry, respectively. **B.** Flow cytometry results showing miCAP percentage in indicated lung tissues (n = 3 or 4, mean ± SEM). Asterisks indicate statistical significance (* p value < 0.05). **C.** Representative IHC images of CAP1- (left) or CAP2-trace (right) mouse lungs after bronchial ligation stained with the lineage trace marker (tdTomato), TrkB, and ERG (scale bar = 100 μm). **D.** A schematic of genetic attenuation of mechanotransduction in CAPs. Control CAP-trace mice or those with a *Cdc42*$^{fl/fl}$ allele were

administrated with three doses of tamoxifen. Cells from control or *Cdc42*$^{CAP-KO}$ lung were used for flow cytometry. **E.** Flow cytometry results showing miCAP percentage in indicated lung tissues (n = 4 or 5, mean ± SEM). NS: no statistical significance.

Figure 4: The emergence of miCAPs requires AT1 cell mechanosensing.

A. A schematic of genetic attenuation of mechanotransduction in AT1s. Control AT1-trace mice or those with a *Cdc42*$^{fl/fl}$ allele were administrated with three doses of tamoxifen, followed by tamoxifen diet. Cells from control or *Cdc42*$^{AT1-KO}$ mouse lungs were isolated and used for scRNA seq analyses at indicated time points. **B.** A UMAP plot of CAPs from control and *Cdc42*$^{AT1-KO}$ mouse lungs. Cells were annotated by cell type. **C.** A bar plot showing percentage of each cell type from control or *Cdc42*$^{AT1-KO}$ mouse lungs. **D.** A dot plot showing expression of indicated genes in each cell type. **E.** A Spearman correlation showing transcriptional similarity between AT1-induced CAPs and ligation-induced miCAPs. **F.** Flow cytometry results showing miCAP percentage in *Cdc42*$^{AT1-KO}$ mouse lungs after three doses of tamoxifen for 14 or 28 days, or control mouse lungs (n = 5, mean ± SEM). Asterisks indicate statistical significance (** p value < 0.01, **** p value < 0.0001). **G.** Representative IHC images of control or *Cdc42*$^{AT1-KO}$ mouse lungs stained with TrkB and ERG (scale bar = 25 μm). **H.** A schematic depicting epithelial-endothelial cell interplay in the context of pulmonary mechanotransduction.

Figure 5: miCAPs are sensitive to mechanical forces.

A. A schematic of reversed bronchial ligation experiment in wildtype mice. Tissues or cells from mouse lungs with restored inflation were used for imaging or flow cytometry, respectively. **B.** Representative micro-CT scan images showing restored lung inflation after clip removal in mouse ligated lungs. **C.** A UMAP plot of CAPs from ligated mouse lung and those after restored lung motion. Cells were annotated by cell type. **D.** Flow cytometry results showing miCAP percentage in indicated lung tissues (n = 4 or 5, mean ± SEM). Asterisks indicate statistical significance (* p value < 0.05). **E.** Representative IHC images of indicated lung tissues stained with TrkB and ERG, a pan endothelial cell marker (scale bar = 25 μm). **F.** A schematic of flow cytometry experiment determining proliferation in cells. EdU water (0.2 g/L) was provided to mice during indicated time periods. Cells from wildtype mouse after reversed bronchial ligation or sham surgery were isolated and used for flow cytometry. **G.** Flow cytometry results showing proliferating EdU^+ cell percentage in indicated EC populations (n = 5, mean ± SEM). Data for Ctrl EC and ECs from ligated mouse

lungs are also shown in Figure 2I. Asterisks indicate statistical significance (* *p* value < 0.05, ** *p* value < 0.01). NS: no statistical significance.

Figure 1

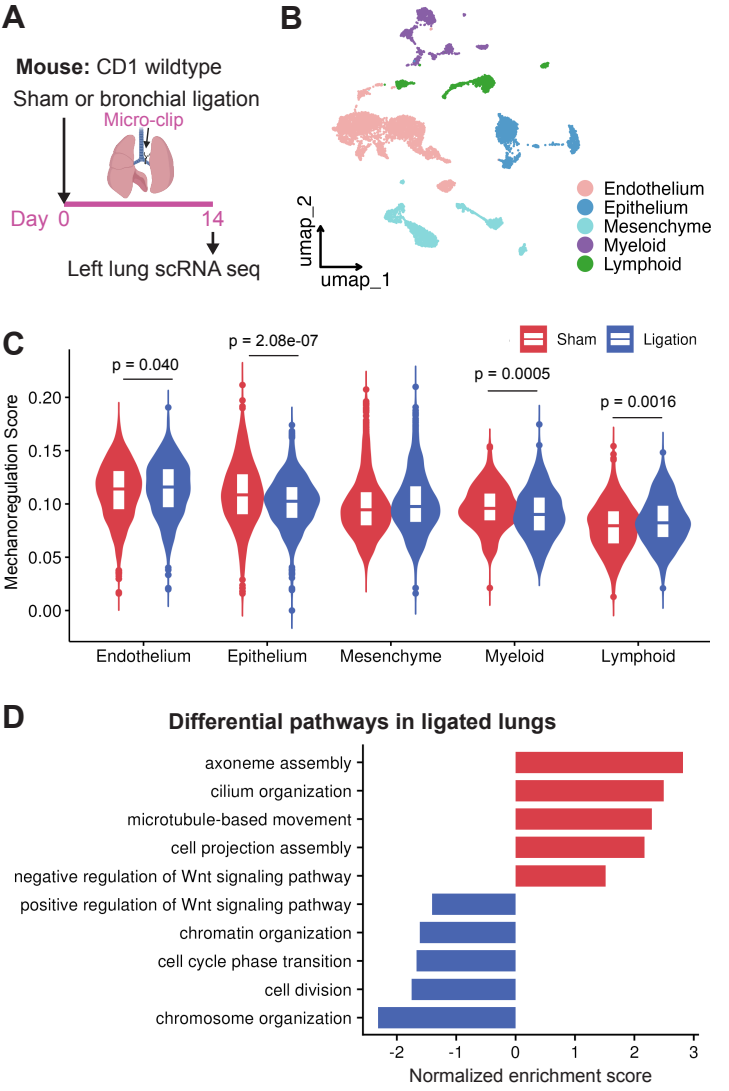
A
Mouse: CD1 wildtype
Sham or bronchial ligation
Micro-clip
Day 0
14
Left lung scRNA seq
B
umap_2
umap_1
Endothelium
Epithelium
Mesenchyme
Myeloid
Lymphoid
C
Sham
Ligation
p = 0.040
p = 2.08e-07
p = 0.0005
p = 0.0016
Mechanoregulation Score
0.20
0.15
0.10
0.05
0.00
Endothelium
Epithelium
Mesenchyme
Myeloid
Lymphoid
D
Differential pathways in ligated lungs
axoneme assembly
cilium organization
microtubule-based movement
cell projection assembly
negative regulation of Wnt signaling pathway
positive regulation of Wnt signaling pathway
chromatin organization
cell cycle phase transition
cell division
chromosome organization
-2
-1
0
1
2
3
Normalized enrichment score

Figure 2

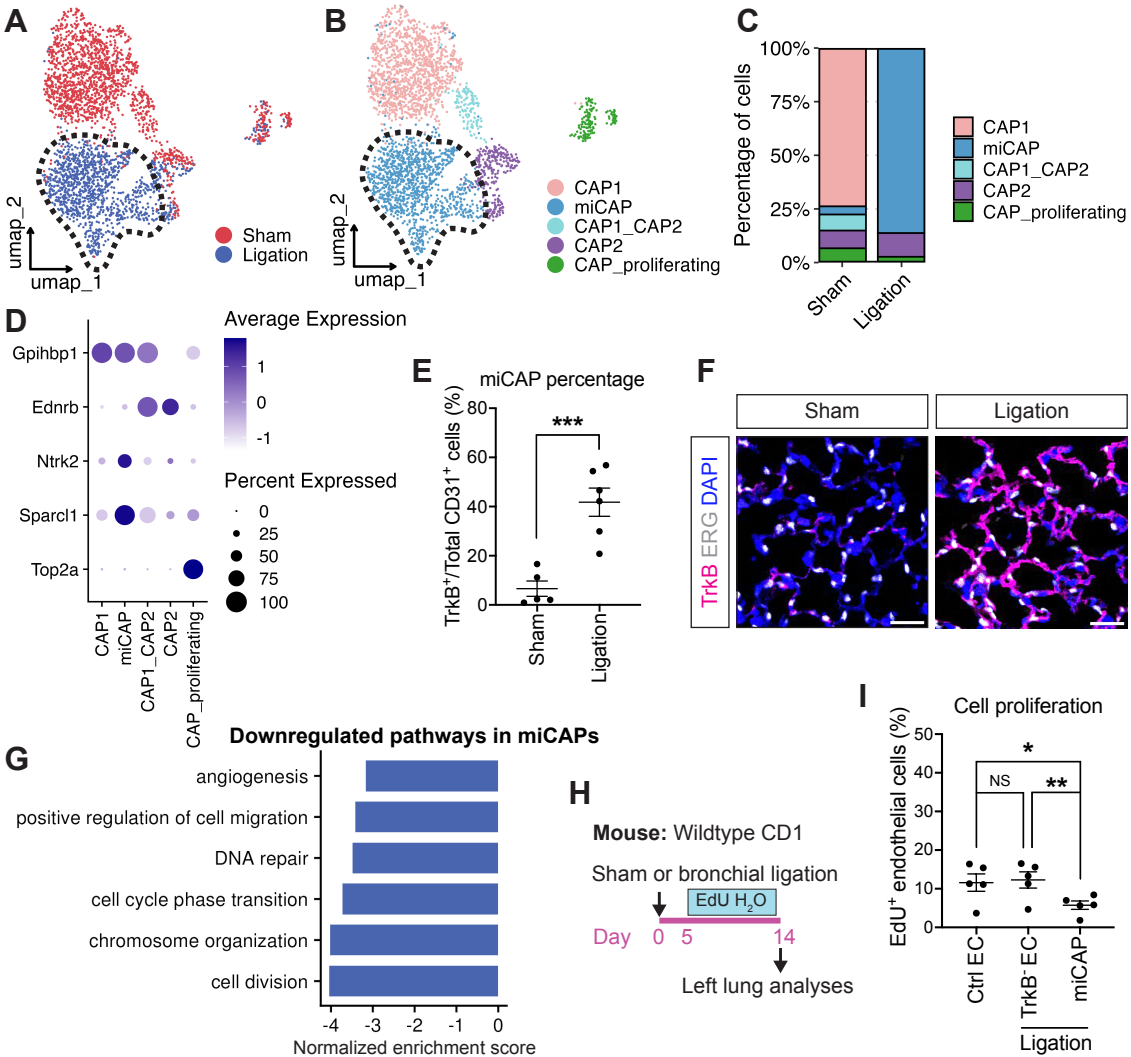
A
umap_2
umap_1
Sham
Ligation
B
umap_2
umap_1
CAP1
miCAP
CAP1_CAP2
CAP2
CAP_proliferating
C
Percentage of cells
100%
75%
50%
25%
0%
Sham
Ligation
CAP1
miCAP
CAP1_CAP2
CAP2
CAP_proliferating
D
Average Expression
1
0
-1
Percent Expressed
0
25
50
75
100
Gpihbp1
Ednrb
Ntrk2
Sparcl1
Top2a
CAP1
miCAP
CAP1_CAP2
CAP2
CAP_proliferating
E
miCAP percentage
TrkB+/Total CD31+ cells (%)
80
60
40
20
0
***
Sham
Ligation
F
Sham
Ligation
TrkB ERG DAPI
G
Downregulated pathways in miCAPs
angiogenesis
positive regulation of cell migration
DNA repair
cell cycle phase transition
chromosome organization
cell division
-4
-3
-2
-1
0
Normalized enrichment score
H
Mouse: Wildtype CD1
Sham or bronchial ligation
EdU H2O
Day 0 5 14
Left lung analyses
I
Cell proliferation
EdU+ endothelial cells (%)
50
40
30
20
10
0
*
NS
**
Ctrl EC
TrkB- EC
miCAP
Ligation

Figure 3

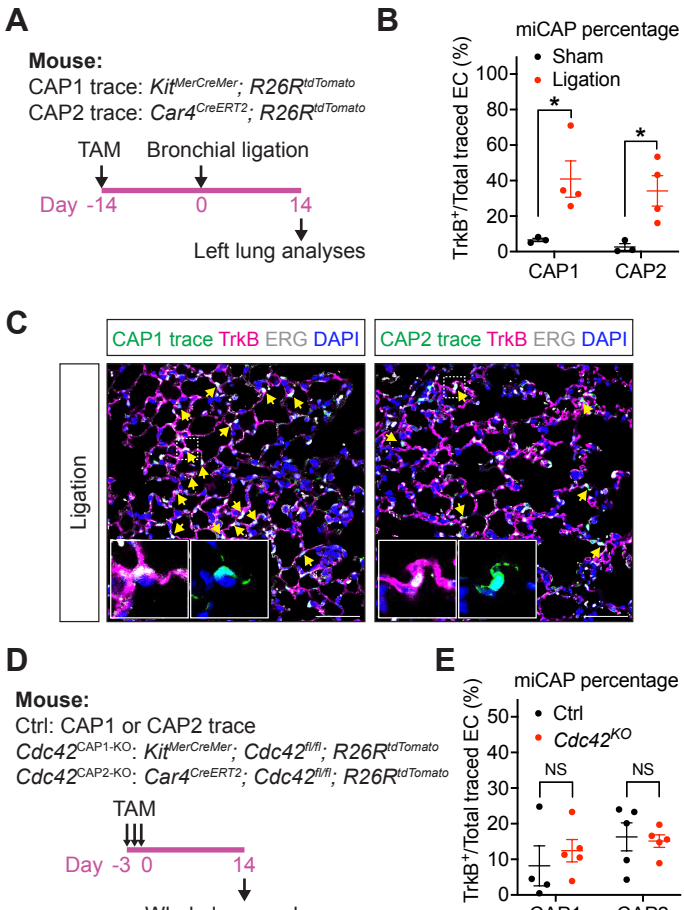
A
Mouse:
CAP1 trace: Kit^MerCreMer; R26R^tdTomato
CAP2 trace: Car4^CreERT2; R26R^tdTomato
TAM
Bronchial ligation
Day -14
0
14
Left lung analyses
B
miCAP percentage
Sham
Ligation
TrkB+/Total traced EC (%)
100
80
60
40
20
0
*
*
CAP1
CAP2
C
CAP1 trace TrkB ERG DAPI
CAP2 trace TrkB ERG DAPI
Ligation
D
Mouse:
Ctrl: CAP1 or CAP2 trace
Cdc42^CAP1-KO: Kit^MerCreMer; Cdc42^fl/fl; R26R^tdTomato
Cdc42^CAP2-KO: Car4^CreERT2; Cdc42^fl/fl; R26R^tdTomato
TAM
Day -3 0
14
Whole lung analyses
E
miCAP percentage
Ctrl
Cdc42^KO
TrkB+/Total traced EC (%)
50
40
30
20
10
0
NS
NS
CAP1
CAP2

Figure 4

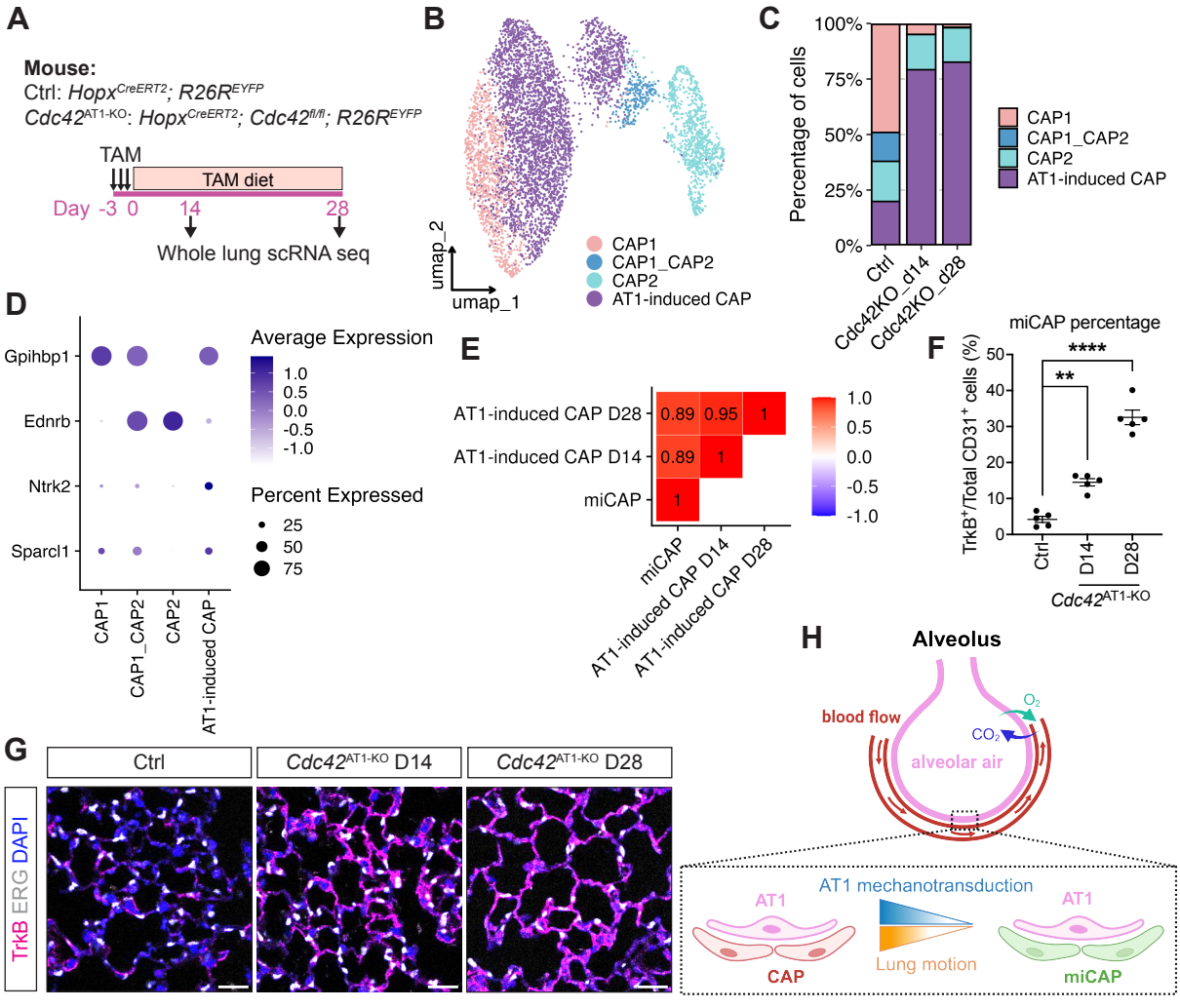
A
Mouse:
Ctrl: Hopx^CreERT2; R26R^EYFP
Cdc42^AT1-KO: Hopx^CreERT2; Cdc42^fl/fl; R26R^EYFP
TAM
TAM diet
Day -3 0 14 28
Whole lung scRNA seq
B
umap_2
umap_1
CAP1
CAP1_CAP2
CAP2
AT1-induced CAP
C
Percentage of cells
100%
75%
50%
25%
0%
Ctrl
Cdc42KO_d14
Cdc42KO_d28
CAP1
CAP1_CAP2
CAP2
AT1-induced CAP
D
Gpihbp1
Ednrb
Ntrk2
Sparcl1
CAP1
CAP1_CAP2
CAP2
AT1-induced CAP
Average Expression
1.0
0.5
0.0
-0.5
-1.0
Percent Expressed
25
50
75
E
AT1-induced CAP D28
AT1-induced CAP D14
miCAP
0.89
0.95
1
0.89
1
1
miCAP
AT1-induced CAP D14
AT1-induced CAP D28
1.0
0.5
0.0
-0.5
-1.0
F
miCAP percentage
TrkB+/Total CD31+ cells (%)
50
40
30
20
10
0
****
**
Ctrl
D14
D28
Cdc42^AT1-KO
G
Ctrl
Cdc42^AT1-KO D14
Cdc42^AT1-KO D28
TrkB ERG DAPI
H
Alveolus
blood flow
O2
CO2
alveolar air
AT1 mechanotransduction
AT1
AT1
CAP
Lung motion
miCAP

Figure 5

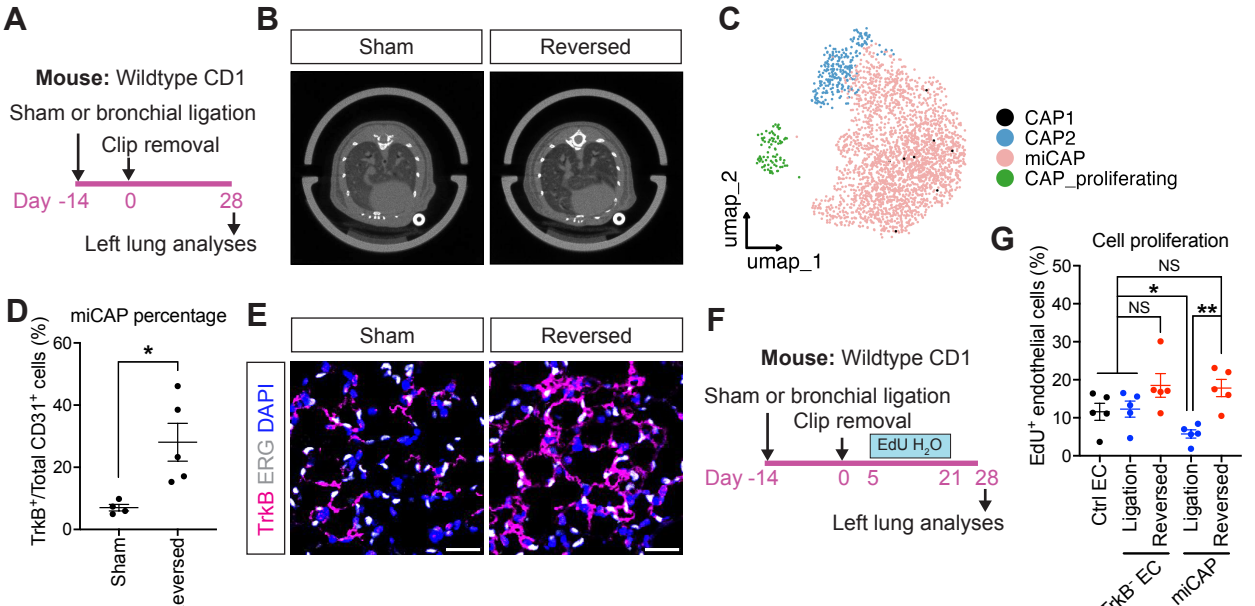
A
Mouse: Wildtype CD1
Sham or bronchial ligation
Clip removal
Day -14
0
28
Left lung analyses
B
Sham
Reversed
C
CAP1
CAP2
miCAP
CAP_proliferating
umap_2
umap_1
D
miCAP percentage
TrkB+/Total CD31+ cells (%)
60
40
20
0
*
Sham
Reversed
E
Sham
Reversed
TrkB ERG DAPI
F
Mouse: Wildtype CD1
Sham or bronchial ligation
Clip removal
EdU H2O
Day -14
0
5
21
28
Left lung analyses
G
Cell proliferation
EdU+ endothelial cells (%)
50
40
30
20
10
0
NS
*
NS
**
Ctrl EC
Ligation
Reversed
Ligation
Reversed
TrkB- EC
miCAP